Non-Hermitian topology in a single driven-dissipative Kerr-Cat qubit

Pei-Rong Han¹, Huiye Qiu¹, Hao-Long Zhang², Wen Ning², Zhen-Biao Yang², and Shi-Biao Zheng^{2*}

¹School of Physics and Mechanical and Electrical Engineering, Longyan University, Longyan 364012, China

²Department of Physics, Fuzhou University, Fuzhou 350108, China

The intriguing physical phenomena associated with exceptional points have established non-Hermitian physics as a frontier of modern research. Recent investigations have extended non-Hermitian physics into the fully quantum domain. However, existing studies predominantly concentrate on discrete-variable quantum systems, while non-Hermitian quantum effects in continuous-variable encoded systems remain largely unexplored. In this work, we investigate the exceptional structure for a driven-dissipative Kerr-cat qubit, realized with a Kerr nonlinear resonator. We find that the dissipation leads to a bidirectional jump between the two basis states of the cat qubit, which is in distinct contrast with the unidirectional jump associated with normal two-level systems. The competition between this jump and a single-photon drive gives arise to the emergence of third-order Liouvillian exceptional points (LEP3s), each corresponds to a crossing point of two lines of LEP2s. We further show that the LEP3 can exhibit the topological character of the Hamiltonian EP3s, which cannot be realized with a single qubit. Our work opens the possibility of realizing non-Hermitian phenomena with continuous-variable quantum systems.

Non-Hermitian physics fundamentally enriches quantum dynamics through exceptional points (EPs)—singular degeneracies where eigenvalues and eigenvectors simultaneously coalesce. A central theme in contemporary studies lies in exploring the topological aspects of non-Hermitian systems, which lead to novel phenomena beyond the Hermitian paradigm [1–17]. Recent advances have realized EPs in the full quantum regime, primarily through two frameworks: measurement-conditioned non-Hermitian dynamics via post-selection [16–21] and intrinsic Liouvillian dynamics incorporating all quantum jumps [22–32]. arising in a non-Hermitian Hamiltonian are termed Hamiltonian EPs (HEPs), while those emerging in a Liouvillian superoperator are termed Liouvillian EPs (LEPs). Although the Liouvillian eigenspectrum can exhibit significantly richer exceptional structures than its non-Hermitian Hamiltonian counterpart, its unique topological features remain largely unexplored. Moreover, prior investigations of LEPs have been mainly restricted to discrete-variable-encoded qubits or gudits [22–32]. The problem remains of how to construct LEPs for continuous-variable-encoded qubits.

In this paper, we investigate the exceptional structure associated with the Liouvillian superoperator for a driven-dissipative cat qubit, which represents one typical example of continuous-variable-encoded qubits [33–39]. The codewords of such a qubit is encoded in the even and odd cat states, defined as $|\mathcal{C}_{\alpha}^{\pm}\rangle = \mathcal{N}_{\alpha}^{\pm}(|\alpha\rangle \pm |-\alpha\rangle)$, where $|\pm\alpha\rangle$ are coherent states and $\mathcal{N}_{\alpha}^{\pm} = 1/\sqrt{2(1\pm e^{-2|\alpha|^2})}$. These two cat states are degenerate eigenstates of a Kerr-nonlinear resonator under two-photon driving. This qubit architecture achieves exponential suppression of bit-flip errors, positioning it as a promising paradigm for fault-tolerant quantum computation. Within the Kerr-

cat qubit framework, we encode the computational basis (Z-basis) using the parity-symmetric cat states $|\mathcal{C}_{\alpha}^{+}\rangle$ (even parity) and $|\mathcal{C}_{\alpha}^{-}\rangle$ (odd parity). The x-axis rotations can be implemented via single-photon driving $H_{1} = \varepsilon(a^{\dagger} + a)$, where ε (real-valued) denotes the tunable driving strength. For large α , the coherent states $|\pm\alpha\rangle$ serve as an approximate X-basis. Figure 1(a) depicts the corresponding Bloch sphere representation of this encoded qubit.

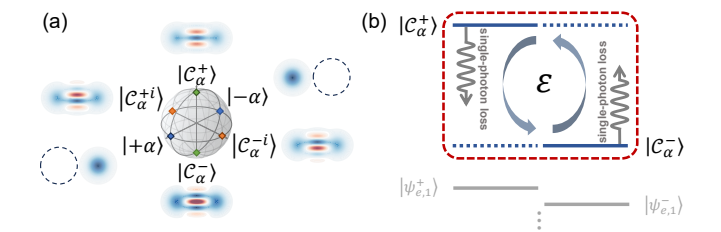


FIG. 1: Kerr-cat qubit representation and effects of single-photon loss. (a) Bloch sphere representation of the protected Kerr-cat qubit in the large- α limit. Colored markers indicate the cardinal points corresponding to the encoded states, alongside their respective Wigner functions. The Z-basis states are defined as $|\pm Z\rangle = |\mathcal{C}_{\alpha}^{\pm}\rangle = \mathcal{N}_{\alpha}^{\pm}(|\alpha\rangle \pm |-\alpha\rangle)$, and the Y-basis states as $|\pm Y\rangle = |\mathcal{C}_{\alpha}^{\mp i}\rangle = (|\mathcal{C}_{\alpha}^{+}\rangle \pm i|\mathcal{C}_{\alpha}^{-}\rangle)/\sqrt{2}$. (b) The dominant source of noise in the resonator is single-photon loss, resulting from coupling to a bath via single-photon exchange. This dissipation induces random bit flips between the states $|\mathcal{C}_{\alpha}^{\pm}\rangle$, as described by $a = \alpha(p|\mathcal{C}_{\alpha}^{-}\rangle\langle\mathcal{C}_{\alpha}^{+}|+p^{-1}|\mathcal{C}_{\alpha}^{+}\rangle\langle\mathcal{C}_{\alpha}^{-}|)$.

The Hermiticity of this system is manifested by the single-photon loss, and the transition between the even and odd cat states is driven by an classical field (Fig. 1(b)). Under the competition between the dissipation and drive, we find that the system exhibits rich exceptional structures, including second-order Liouvillian exceptional lines (LEP2 lines) and third-order LEPs (LEP3s). We further characterize the topological nature of each LEP3 by computing the winding number of the

^{*}E-mail: fjqiqo@fzu.edu.cn

resultant vector [40].

Under single-photon loss with dissipation rates κ , the system's evolution is governed by the Lindblad master equation

$$\dot{\rho} \equiv \mathcal{L}(\rho) = -i[H, \rho] + \kappa (a\rho a^{\dagger} - \frac{1}{2}a^{\dagger}a\rho - \frac{1}{2}\rho a^{\dagger}a), \quad (1)$$

where ρ is the density operator, and $a^{\dagger}(a)$ is the creation (annihilation) operator for the Kerr-nonlinear resonator. The dynamics can be fully captured by the Liouvillian superoperator \mathcal{L} . In the frame rotating at the driving frequency,

$$H = \Delta a^{\dagger} a - K a^{\dagger 2} a^2 + P (a^{\dagger 2} + a^2) + \varepsilon (a^{\dagger} + a),$$
 (2)

where Δ is the detuning between the drive and resonator, K is the Kerr coefficient and P is the amplitude of the two-photon driving. For simplicity and without loss of generality, we restrict both K and P to be positive and real throughout this paper, which implies that α is likewise real. When $\Delta = \varepsilon = 0$, the coherent states $|\pm\alpha\rangle$ are two degenerate eigenstates of the system Hamiltonian with the eigenvalue P^2/K , where $\alpha = \sqrt{P/K}$. In such

a degenerate subspace, any state can also be expressed in terms of the even and odd cat states $|\mathcal{C}_{\alpha}^{\pm}\rangle$, which are orthogonal to each other and thus form the basis for a qubit. The energy gap between these degenerate eigenstates and their nearest eigenstates is $4K|\alpha|^2$. When the single-photon driving strength, dissipative rate, and the detuning are much smaller than this gap, the system is approximately restricted in the subspace of the cat qubit.

To investigate the Liouvillian spectrum and LEPs, we employ a vectorized representation to express the Liouvillian superoperator in matrix form. In this representation, Eq. (1) takes the form $\dot{\boldsymbol{V}}(t) = \mathcal{L}_{\text{matrix}} \boldsymbol{V}(t)$, where \boldsymbol{V} is a vectorized density matrix and $\mathcal{L}_{\text{matrix}}$ is the matrix form of the Liouvillian superoperator \mathcal{L} , given by

$$\mathcal{L}_{\text{matrix}} = -i \left(H \otimes I - I \otimes H^{\top} \right)$$

$$+ \left[\Gamma_a \otimes \Gamma_a^* - \frac{\Gamma_a^{\dagger} \Gamma_a \otimes I}{2} - \frac{I \otimes \Gamma_a^{\top} \Gamma_a^*}{2} \right],$$
(3)

where \otimes represents Kronecker product operation, \top represents the transpose, * represents the complex conjugate and $\Gamma_a = \sqrt{\kappa}a$. Projecting \mathcal{L} into the subspace spanned by $\{|\mathcal{C}_{\alpha}^{+}\rangle, |\mathcal{C}_{\alpha}^{-}\rangle\}$ yields a 4×4 matrix representation,

$$\mathcal{L}_{\text{matrix}} = \begin{pmatrix}
-\alpha^2 \kappa p^2 & i\alpha \varepsilon p_1^+ & -i\alpha \varepsilon p_1^+ & \alpha^2 \kappa p^{-2} \\
i\alpha \varepsilon p_1^+ & \alpha^2 (-\frac{\kappa}{2} p_2^+ + i\Delta p_2^-) & \alpha^2 \kappa & -i\alpha \varepsilon p_1^+ \\
-i\alpha \varepsilon p_1^+ & \alpha^2 \kappa & \alpha^2 (-\frac{\kappa}{2} p_2^+ - i\Delta p_2^-) & i\alpha \varepsilon p_1^+ \\
\alpha^2 \kappa p^2 & -i\alpha \varepsilon p_1^+ & i\alpha \varepsilon p_1^+ & -\alpha^2 \kappa p^{-2}
\end{pmatrix},$$
(4)

where $p_j^{\pm} = p^{-j} \pm p^j$, with $p = \mathcal{N}_{\alpha}^{+}/\mathcal{N}_{\alpha}^{-}$. The derivation relies on the relations $a|\mathcal{C}_{\alpha}^{\pm}\rangle = \alpha p^{\pm 1}|\mathcal{C}_{\alpha}^{\mp}\rangle$ and $a^{\dagger}|\mathcal{C}_{\alpha}^{\pm}\rangle = \alpha p^{\mp 1}|\mathcal{C}_{\alpha}^{\mp}\rangle$ within the subspace. Assuming $\mathcal{L}_{\text{matrix}}$ is diagonalizable, let E_i and V_i denote its eigenvalues and corresponding eigenmatrices, respectively. The time evolution of V(t) is then expressed as

$$\mathbf{V}(t) = \sum_{i} c_{i} \exp(E_{i}t) \mathbf{V}_{i}. \tag{5}$$

Using Cardano's method, the eigenvalues of $\mathcal{L}_{\mathrm{matrix}}$ are explicitly given by

$$E_1 = 0, (6)$$

$$E_2 = -\frac{2}{3}\kappa\alpha^2 p_2^+ + (\eta_+ + \eta_-),\tag{7}$$

$$E_3 = -\frac{2}{3}\kappa\alpha^2 p_2^+ + \left(e^{i\frac{2\pi}{3}}\eta_+ + e^{-i\frac{2\pi}{3}}\eta_-\right),\tag{8}$$

$$E_4 = -\frac{2}{3}\kappa\alpha^2 p_2^+ + \left(e^{-i\frac{2\pi}{3}}\eta_+ + e^{i\frac{2\pi}{3}}\eta_-\right),\tag{9}$$

where
$$\eta_{\pm} = \sqrt[3]{q \pm \sqrt{q^2 - m^3}}$$
 with

$$q = \frac{\alpha^4}{216} \left[-\alpha^2 (36\Delta^2 + \kappa^2) p_6^+ + 72\varepsilon^2 p_4^+ + (36\Delta^2 \alpha^2 + 576\varepsilon^2 + 33\kappa^2 \alpha^2) p_2^+ + 1008\varepsilon^2 \right],$$

and

$$m = \frac{\alpha^2}{36} [\alpha^2 (12\Delta^2 - \kappa^2) p_4^+ + 48\varepsilon^2 p_2^+ - 24\Delta^2 \alpha^2 + 96\varepsilon^2 - 14\alpha^2 \kappa^2].$$

The eigenvalues are characterized by a vanishing E_1 (whose eigenvector corresponds to the steady state ρ_{ss}), a strictly real E_2 , and a complex conjugate pair E_3 , E_4 . Single-photon driving induces a topological transition where the original LEP2 at $|\Delta| = \kappa/p_2^-$ when $\varepsilon = 0$ splits into two daughter exceptional points of identical order or turns to a LEP3, as shown in Fig. 2(a). The

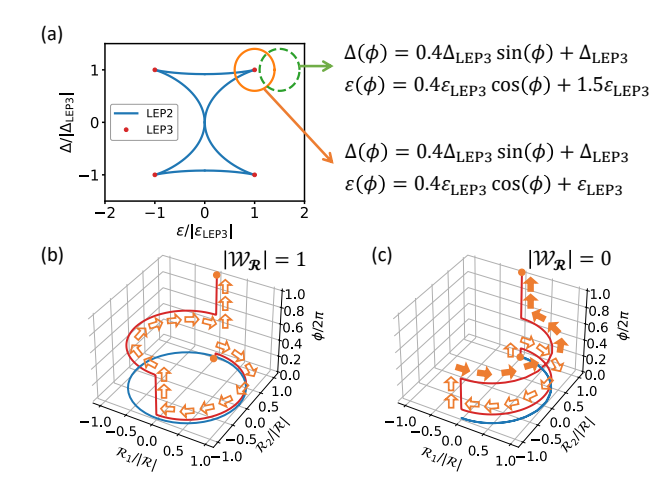


FIG. 2: Topology of the Liouvillian superoperator. (a) Solid curves depict second-order Liouvillian exceptional points (LEP2s), along which pairs of eigenvectors coalesce. Red dots indicate third-order exceptional points (LEP3s). The solid orange circle (enclosing a single LEP3) and dashed green circle (excluding LEP3s) indicate Winding number calculation contours in parameter space. (b)(c) Winding number of the resultant vector. (b) Trajectory of the normalized resultant vector $\mathcal{R}_{N} \equiv (\mathcal{R}_{1} + i\mathcal{R}_{2})/|\mathcal{R}|$ under parameter variation along \mathcal{C}_{ϕ} . The x, y and z axes represent $\mathcal{R}_1/|\mathcal{R}|$, $\mathcal{R}_2/|\mathcal{R}|$ and $\phi/2\pi$, respectively. The red trajectory shows the evolution of \mathcal{R}_1 and \mathcal{R}_2 as ϕ varies. Its projection onto the rescaled \mathcal{R}_1 - \mathcal{R}_2 plane forms a closed circle (solid blue line), indicating a topological winding number $|\mathcal{W}_{\mathcal{R}}| = 1$. (c) In contrast, when the projection does not form a closed circle, the winding number is $|\mathcal{W}_{\mathcal{R}}| = 0$. The starting point and end point are marked by solid orange dots. Solid arrows indicate counterclockwise winding, while hollow arrows indicate clockwise winding.

LEP3s appear at

$$|\varepsilon_{\text{LEP3}}| = \frac{\sqrt{6}\kappa}{18} \frac{\alpha (p^4 + 1)^{3/2}}{p (p^2 + 1)^2},$$
 (10)

$$|\Delta_{\text{LEP3}}| = \frac{\sqrt{3}\kappa}{18} \frac{(p^4 + 6p^2 + 1)^{3/2}}{(p^2 - 1)(p^2 + 1)^2}.$$
 (11)

Recently, it was predicted that HEPs can emerge in a Kerr cat qubit that is subjected to dephasing, but is free of dissipation [41], which is the dominant decoherence source of the Kerr-cat qubit realized in the experiment reported in Ref. [33].

The resulting exceptional structure is similar with that revealed in Ref. [27], both featuring EP2 lines intersecting at EP3 vertices. Crucially, their physical origins differ fundamentally. For Kerr-cat qubits, single-photon dissipation induces bidirectional quantum jumps between even- and odd-parity cat states. This effect is analogous to a quantum jump operator represented by σ_x in a conventional qubit. The exceptional structures illustrated in Fig. 2(a) originate from this bidirectionality of quantum jumps, whereas those reported in Ref. [27] arise from unidirectional quantum jumps from the excited to the ground state.

Consider their apparent similarity, these configurations exhibit analogous topological properties. The topological invariant associated with the exceptional structure can be quantified by the winding number of the resultant vector \mathcal{R} [40],

$$W_{\mathcal{R}} = \frac{1}{2\pi} \oint_{\mathcal{C}_{\phi}} \frac{1}{\|\mathcal{R}\|^2} \left(\mathcal{R}_1 \frac{\partial \mathcal{R}_2}{\partial \phi} - \mathcal{R}_2 \frac{\partial \mathcal{R}_1}{\partial \phi} \right) d\phi, \quad (12)$$

where \mathcal{C}_{ϕ} denotes a closed contour in ε - Δ parameter space and is parameterized by ϕ . The resultant of two polynomials is the determinant of their Sylvester matrix, vanishing if and only if the polynomials possess a common root. Up to a nonzero multiplicative factor, the characteristic polynomial $P(E) \equiv \det[\mathcal{L}_{\text{matrix}} - E\mathbb{I}]$ of $\mathcal{L}_{\text{matrix}}$ can be written as $P(E) = \prod_{i=1}^4 (E-E_i)$. Since the steady state and its corresponding eigenvalue do not contribute to the formation of exceptional points, the winding number is governed solely by the remaining three eigenvalues. We therefore factor out the steady-state eigenvalue and consider the cubic polynomial formed by the other three: $\tilde{P}(E) = (E - E_2)(E - E_3)(E - E_4)$. This leads to the following explicit expressions for the resultants \mathcal{R}_1 and \mathcal{R}_2 in terms of eigenvalues E_i

$$\mathcal{R}_1 = -(E_2 - E_3)^2 (E_2 - E_4)^2 (E_3 - E_4)^2, \qquad (13)$$

and

$$\mathcal{R}_{2} = -8 \left(E_{2} + E_{3} - 2E_{4} \right) \left(E_{2} + E_{4} - 2E_{3} \right) \left(E_{3} + E_{4} - 2E_{2} \right). \tag{14}$$

As established in Ref. [40], a value of $|\mathcal{W}_{\mathcal{R}}| = 1$ signifies that the region enclosed by the contour contains a LEP3, where $\mathcal{R}_1 = \mathcal{R}_2 = 0$. Figure 2(b) and (c) illustrate the behavior of the rescaled \mathcal{R}_1 and \mathcal{R}_2 as functions of ϕ for two different contours \mathcal{C}_{ϕ} : one encircling only a LEP3, and one excluding the LEP3. The results demonstrate that when a LEP3 is enclosed, $|\mathcal{W}_{\mathcal{R}}| = 1$. Therefore, the LEP3 shares the same topological properties as a HEP3 reported in Ref. [16].

It is necessary to show to what extent the system can be restricted in the subspace of Kerr-cat qubit during the state evolution. To do so, we respectively calculate the density matrix (σ) evolved under the effective Liouvillian dynamics of Eq. (5) and that (ρ) governed by the original master equation of Eq. (1). The validity of the approximation is quantified by the fidelity, defined as $F(\rho,\sigma) = (\text{Tr}\sqrt{\sqrt{\rho}\sigma\sqrt{\rho}})^2$. The fidelities for different initial states, as functions of the detuning and time, are presented in Fig. 3. In the simulation, we use the parameters reported in the experiment of Ref. [33]: $K/2\pi = 6.7$ MHz, $P/2\pi = 15.5$ MHz, and $\kappa = 1/15.5$ MHz. The resulting coherent-state amplitude is $\alpha \approx 1.52$. ε is set to $0.74 \times 2\pi$ MHz, which corresponds to the single-photon drive strength used for implementing the X-rotation in the experiment reported in Ref. [33]. As shown, the two dynamical evolutions exhibit excellent agreement over the selected parameter range, with fidelity exceeding 0.930. The fidelity asymptotically approaches 1 as the

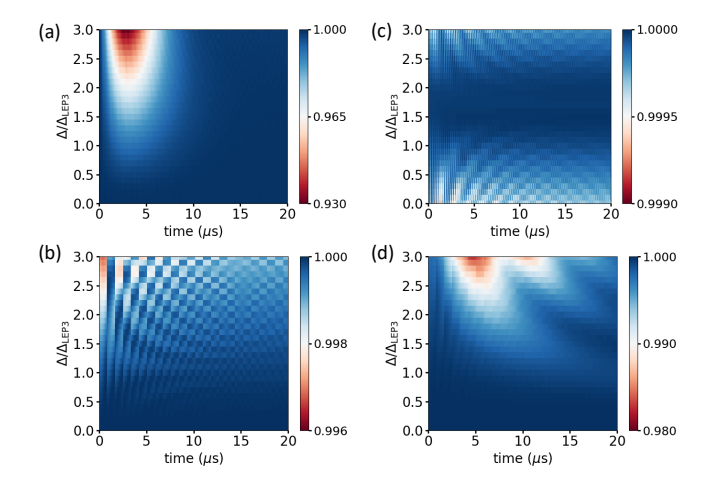


FIG. 3: Validation of the Liouvillian dynamics. Color represents the fidelity $F(\rho_{\rm H},\rho_{\rm L})$ between states evolved under the Lindblad master equation and the Liouvillian approximation. (a) Initial state $|\mathcal{C}_{\alpha}^{+}\rangle$ with $\varepsilon/2\pi=0.74$ MHz. (b) Initial state $|\mathcal{C}_{\alpha}^{+}\rangle$ without single-photon driving. (c) Initial state $|\alpha\rangle$ with $\varepsilon/2\pi=0.74$ MHz. (d) Initial state $|\alpha\rangle$ without single-photon driving. Numerical parameters are taken from Ref. [33]: $K/2\pi=6.7$ MHz, $\kappa=1/15.5$ MHz, $|\alpha|^2=2.3$.

system relaxes to its steady state with increasing time. Minor deviations originate primarily from the detuning $\Delta a^{\dagger}a$ and the single-photon driving $\varepsilon(a^{\dagger}+a)$, which are not fully captured in the effective Liouvillian description.

To clarify the underlying mechanisms, we analyze the individual effects of the detuning and the single-photon driving. The detuning term $\Delta a^{\dagger}a$ in Eq. (2) effectively

lifts the degeneracy of the even and odd cat states. This is due to the fact they have slightly different photon numbers, given by $\alpha^2 p^2$ and α^2/p^2 , respectively. Consequently, the expectation values of this term are different for these two cat states. Furthermore, this term can induce transitions from these cat states to other eigenstates of the Hamiltonian with $\Delta = \varepsilon = 0$. The single-photon driving and dissipation can also make the system jump out of the subspace spanned by the cat qubit. In principle, these unwanted effects can be mitigated by decreasing the values of the parameters κ , Δ , and ε .

In summary, we have investigated the exceptional structure and topological properties of a Kerr-cat qubit realized in a driven-dissipative Kerr resonator. We have discovered that the LEP3 shares the same topological characteristics as a HEP3, as captured by the winding number $\mathcal{W}_{\mathcal{R}}$ of the resultant vector. Using experimentally relevant parameters, our numerical simulations validate the effectiveness of the Liouvillian dynamics, confirming the experimental feasibility of the predicted exceptional structure. The exclusive presence of LEPs indicates that they are solely induced by bidirectional quantum jumps, underscoring the fundamental distinction between LEPs and HEPs in the quantum regime. Our work paves the way for exploration of exotic features in NH continuous-variable-encoded qubits.

This work was supported by the National Natural Science Foundation of China (Grant Nos. 12505021, 12474356, 12274080, 12475015, 12505016), the Natural Science Foundation of Fujian Province (Grant Nos. 2025J01383, 2025J01465) and the Research Startup Funds of Longyan University (LB2025002).

- C. Dembowski, H.-D. Gräf, H. L. Harney, A. Heine, W. D. Heiss, H. Rehfeld, and A. Richter, Experimental observation of the topological structure of exceptional points, Phys. Rev. Lett. 86, 787-790 (2001).
- [2] H. Zhou, C. Peng, Y. Yoon, C. W. Hsu, K. A. Nelson, L. Fu, J. D. Joannopoulos, M. Soljačić, and B. Zhen, Observation of bulk Fermi arc and polarization half charge from paired exceptional points, Science 359, 1009–1012 (2018).
- [3] A. Cerjan, S. Huang, M. Wang, K. P. Chen, Y. Chong, and M. C. Rechtsman, Experimental realization of a Weyl exceptional ring, Nat. Photon. 13, 623–628 (2019).
- [4] J. J. Liu, Z. W. Li, Z. G. Chen, W. Tang, A. Chen, B. Liang, G. Ma, and J.-C. Cheng, Experimental realization of Weyl exceptional rings in a synthetic threedimensional non-Hermitian phononic crystal, Phys. Rev. Lett. 129, 084301 (2022).
- [5] B. Zhen, C. W. Hsu, Y. Igarashi, Lu, L., I. Kaminerv, A. Pick, S.-L. Chua, J. D. Joannopoulos, and M. Soljačić, Spawning rings of exceptional points out of Dirac cones, Nature (London) 525, 354–358 (2015).
- [6] K. Wang, A. Dutt, K. Y. Yang, C. C. Wojcik, J. Vučković, and S. Fan, Generating arbitrary topological windings of a non-Hermitian band, Science 371, 1240–

- 1245 (2021).
- [7] K. Wang, A. Dutt, C. C. Wojcik, and S. Fan, Topological complex-energy braiding of non-Hermitian bands, Nature **598**, 59–64 (2021).
- [8] Q.Zhang, Y. Li, H. Sun, X. Liu, L. Zhao, X. Feng, X. Fan, and C. Qiu, Observation of acoustic non-Hermitian Bloch braids and associated topological phase transitions, Phys. Rev. Lett. 130, 017201 (2023).
- [9] W. Tang, K. Ding, and G. Ma, Direct measurement of topological properties of an exceptional parabola, Phys. Rev. Lett. 127, 034301 (2021).
- [10] R. Su et al. Direct measurement of a non-Hermitian topological invariant in a hybrid light-matter system. Sci. Adv. 7, eabj8905 (2021).
- [11] W. Zhang, X. Ouyang, X. Huang, X. Wang, H. Zhang, Y. Yu, X. Chang, Y. Liu, D.-L. Deng, and L.-M. Duan, Observation of non-Hermitian topology with nonunitary dynamics of solid-state spins, Phys. Rev. Lett. 127, 090501 (2021).
- [12] M.-M. Cao, K. Li, W.-D. Zhao, W.-X. Guo, B.-X. Qi, X.-Y. Chang, Z.-C. Zhou, Y. Xu, and L.-M. Duan, Probing complex-energy topology via non-Hermitian absorption spectroscopy in a trapped ion simulator, Phys. Rev. Lett. 130, 163001 (2023).

- [13] Y. Wu, Y. Wang, X. Ye, W. Liu, C.-K. Duan, Y. Wang, X. Rong, and J. Du, Observation of the knot topology of non-Hermitian systems in a single spin, Phys. Rev. A 108, 052409 (2023).
- [14] W. Tang, X. Jiang, K. Ding, Y.-X. Xiao, Z.-Q. Zhang, C. T. Chan, and G. Ma, Exceptional nexus with a hybrid topological invariant, Science 370, 1077–1080 (2020).
- [15] W. Tang, K. Ding, and G. Ma, Realization and topological properties of third-order exceptional lines embedded in exceptional surfaces, Nat. Commun. 14, 6660 (2023).
- [16] P.-R. Han, W. Ning, X.-J. Huang, R.-H. Zheng, S.-B. Yang, F. Wu, Z.-B. Yang, Q.-P. Su, C.-P. Yang, and S.-B. Zheng, Measuring topological invariants for higher-order exceptional points in quantum three-mode systems, Nat. Commun. 15, 10293 (2024).
- [17] H.-L. Zhang, P.-R. Han, X.-J. Yu, S.-B. Yang, J.-H. Lü, W Ning, C.-P. Yang, Z.-B. Yang, Q.-P. Su, and S.-B. Zheng, Implementation and topological characterization of Weyl exceptional rings in quantum-mechanical systems, Sci. Bull. 70, 2446 (2025).
- [18] M. Naghiloo, M. Abbasi, Y. N. Joglekar, and K. W. Murch, Quantum state tomography across the exceptional point in a single dissipative qubit, Nat. Phys. 15, 1232 (2019).
- [19] Z. Wang, Z. Xiang, T. Liu, X. Song, P. Song, X. Guo, L. Su, H. Zhang, Y. Du, and D. Zheng, Observation of the exceptional point in superconducting qubit with dissipation controlled by parametric modulation, Chin. Phys. B 30, 100309 (2021).
- [20] M. Abbasi, W. Chen, M. Naghiloo, Y. N. Joglekar, K. W. Murch, Topological Quantum State Control through Exceptional-Point Proximity, Phys. Rev. Lett. 128, 160401 (2022).
- [21] P. R. Han, F. Wu, X. J. Huang, H. Z. Wu, C. L. Zou, W. Yi, M. Zhang, H. Li, K. Xu, D. Zheng, H. Fan, J. Wen, Z. B. Yang, and S. B. Zheng, Exceptional entanglement phenomena: Non-Hermiticity meeting non-classicality, Phys. Rev. Lett. 131, 260201 (2023).
- [22] F. Minganti, A. Miranowicz, R. W. Chhajlany, and F. Nori, Quantum exceptional points of non-Hermitian Hamiltonians and Liouvillians: The effects of quantum jumps, Phys. Rev. A 100, 062131 (2019).
- [23] I. I. Arkhipov, A. Miranowicz, F. Minganti, and F. Nori, Quantum and semiclassical exceptional points of a linear system of coupled cavities with losses and gain within the Scully-Lamb laser theory, Phys. Rev. A 101, 013812 (2020).
- [24] F. Minganti, A. Miranowicz, R. W. Chhajlany, I. I. Arkhipov, and F. Nori, Hybrid-liouvillian formalism connecting exceptional points of non hermitian hamiltonians and liouvillians via postselection of quantum trajectories, Phys. Rev. A 101, 062112 (2020).
- [25] I. I. Arkhipov, A. Miranowicz, F. Minganti, and F. Nori, Liouvillian exceptional points of any order in dissipative linear bosonic systems: Coherence functions and switching between PT and anti-PT symmetries, Phys. Rev. A 102, 033715 (2020).
- [26] S. Khandelwal, N. Brunner, and G. Haack, Signatures of Liouvillian Exceptional Points in a Quantum Thermal Machine, PRX Quantum 2, 040346 (2021).
- [27] K. Sun, and W. Yi, Encircling the Liouvillian exceptional

- points: a brief review, AAPPS Bull. 34, 22 (2024).
- [28] W. Chen, M. Abbasi, Y. N. Joglekar, and K. W. Murch, Quantum Jumps in the Non-Hermitian Dynamics of a Superconducting Qubit, Phys. Rev. Lett. 127, 140504 (2021).
- [29] W. Chen, M. Abbasi, B. Ha, S. Erdamar, Y. N. Joglekar, and K. W. Murch, Decoherence-Induced Exceptional Points in a Dissipative Superconducting Qubit, Phys. Rev. Lett. 128, 110402 (2022).
- [30] S. Abo, P. Tulewicz, K. Bartkiewicz, Ş. K. Özdemir, and A. Miranowicz, Experimental Liouvillian exceptional points in a quantum system without Hamiltonian singularities, New J. Phys. 26, 123032 (2024).
- [31] J.-W. Zhang, J.-Q. Zhang, G.-Y. Ding, J.-C. Li, J.-T. Bu, B. Wang, L.-L. Yan, S.-L. Su, L. Chen, F. Nori, Ş. K. Özdemir, F. Zhou, H. Jing, and M. Feng, Dynamical control of quantum heat engines using exceptional points, Nat. Commun. 13, 6225 (2022).
- [32] J.-T. Bu, J.-Q. Zhang, G.-Y. Ding, J.-C. Li, J.-W. Zhang, B. Wang, W.-Q. Ding, W.- F. Yuan, L. Chen, Ş. K. Özdemir, F. Zhou, H. Jing, and M. Feng, Enhancement of Quantum Heat Engine by Encircling a Liouvillian Exceptional Point, Phys. Rev. Lett. 130, 110402 (2023).
- [33] A. Grimm, N. E. Frattini, S. Puri, S. O. Mundhada, S. Touzard, M. Mirrahimi, S. M. Girvin, S. Shankar, M. H. Devoret, Stabilization and operation of a Kerr-cat qubit, Nature 584, 205–209 (2020).
- [34] Z. Leghtas, S. Touzard, I. M. Pop, A. Kou, B. Vlastakis, A. Petrenko, K. M. Sliwa, A. Narla, S. Shankar, M. J. Hatridge, M. Reagor, L. Frunzio, R. J. Schoelkopf, M. Mirrahimi, M. H. Devoret, Confining the state of light to a quantum manifold by engineered two-photon loss, Science 347, 853-857(2015).
- [35] S. Puri, S. Boutin, A. Blais, Engineering the quantum states of light in a Kerr-nonlinear resonator by twophoton driving, npj Quantum Inf. 3, 18 (2017).
- [36] B. Vlastakis, G. Kirchmair, Z. Leghtas, S. E. Nigg, L. Frunzio, S. M. Girvin, M. Mirrahimi, M. H. Devoret, R. J. Schoelkopf, Deterministically Encoding Quantum Information Using 100-Photon Schrödinger Cat States, Science 342, 607-610(2013).
- [37] S. Puri, A. Grimm, P. Campagne-Ibarcq, A. Eickbusch, K. Noh, G. Roberts, L. Jiang, M. Mirrahimi, M. H. Devoret, S. M. Girvin, Stabilized Cat in a Driven Nonlinear Cavity: A Fault-Tolerant Error Syndrome Detector, Phys. Rev. X 9, 041009 (2019).
- [38] H. Goto, Universal quantum computation with a nonlinear oscillator network, Phys. Rev. A 93, 050301 (2016).
- [39] F. Minganti, N. Bartolo, J. Lolli, W. Casteels, C. Ciuti, Exact results for Schrödinger cats in driven-dissipative systems and their feedback control, Sci. Rep. 6, 26987 (2016).
- [40] P. Delplace, Tsuneya Yoshida, and Y. Hatsugai, Symmetry-Protected Multifold Exceptional Points and Their Topological Characterization, Phys. Rev. Lett. 127, 186602 (2021).
- [41] K.-X. Yan, Z.C. Shi, Y.H. Chen, and Y. Xia, Controllable Non-Hermitianity in Continuous-Variable Qubits, https://arxiv.org/abs/2511.04110v1.